12-2019

Enabling High Quality Oxygen Measurements during Robotic Based Studies of Ocean Ecological and Biogeochemical Processes

Brianna A. Alanis
The University of Texas Rio Grande Valley

ENABLING HIGH QUALITY OXYGEN MEASUREMENTS DURING ROBOTIC BASED STUDIES OF OCEAN ECOLOGICAL AND BIOGEOCHEMICAL PROCESSES

A Thesis

by

BRIANNA A. ALANIS

Submitted to the Graduate College of
The University of Texas Rio Grande Valley
In partial fulfillment of the requirements for the degree of

MASTER OF SCIENCE

December 2019

Major Subject: Ocean, Coastal and Earth Science

ENABLING HIGH QUALITY OXYGEN MEASUREMENTS DURING ROBOTIC BASED STUDIES OF OCEAN ECOLOGICAL AND BIOGEOCHEMICAL PROCESSES

A Thesis
by
BRIANNA A. ALANIS

COMMITTEE MEMBERS

Dr. John Breier
Chair of Committee

Dr. David Hicks
Committee Member

Dr. Owen Temby
Committee Member

December 2019

ABSTRACT

Alanis, Brianna A., Enabling High Quality Oxygen Measurements during Robotic Based Studies of Ocean Ecological and Biogeochemical Processes. Master of Science (MS), December, 2019, 45 pp., 5 tables, 14 figures, reference, 45 titles.

Dissolved oxygen is an essential parameter necessary for understanding marine ecological and biogeochemical processes. New robotic vehicles and autonomous platforms are being applied to an even wider range of ecological and biogeochemical studies. Thus, arises the opportunity for matching the best possible oxygen sensing techniques and methods to these new platforms. In so doing, we can enable both more targeted and higher resolution oxygen measurements than previously possible and potentially use oxygen measurements for a wider range of applications, including *in situ* incubation experiments and primary productivity measurements. This thesis tested three different oxygen sensors in a trade study for stability, accuracy, precision, drift and detection limits. This thesis also conducted an iron oxidation field application study in order to fully understand the obstacles and difficulties that occur when utilizing and deploying oxygen sensors. The iron oxidation field study determined an average dissolved iron half life of approximately 4.2 hrs. The kinetic rate of iron oxidation at Lo'ihi was then compared to other known sites. The comparison revealed Lo'ihi to have a slower oxidation rate than most other sites. This is likely due to the fact that Lo'ihi is located in the oxygen minimum zone.

DEDICATION

It is my warmest regards to dedicate this work to my family. I could not have completed my master's degree without your love and support.

Thank you for always encouraging me to follow my passions.

ACKNOWLEDGMENTS

I am truly thankful for my committee chair and advisor, Dr. John Breier, for his patience and guidance. I would also like to thank my other committee members, Dr. Owen Temby and Dr. David Hicks, for their help and advisement in my thesis. Additionally, I am grateful to the SUBSEA science team and crew of the E/V Nautilus for their help during data collection. This research used data provided by the Ocean Exploration Trust's *Nautilus* Exploration Program, Cruise NA100. This publication was made possible by the *National Oceanic and Atmospheric Administration, Office of Education Educational Partnership Program award* (NA16SEC4810009). Its contents are solely the responsibility of the award recipient and do not necessarily represent the official views of the *U.S. Department of Commerce, National Oceanic and Atmospheric Administration*. Any opinions, findings, conclusions, or recommendations expressed in this publication are those of the author and do not necessarily reflect the view of the *U.S. Department of Commerce, National Oceanic and Atmospheric Administration*.

Thank you.

TABLE OF CONTENTS

LIST OF TABLES

Page

LIST OF FIGURES

Page

CHAPTER I

INTRODUCTION

Dissolved oxygen is a fundamental parameter necessary for understanding marine ecological and biogeochemical processes. There have been numerous papers written on the significance of dissolved oxygen concerning biogeochemical processes (Johnson et al., n.d.; Ulloa et al., 2012). New robotic vehicles and autonomous platforms, such as the *Clio* profiler Autonomous Underwater Vehicle (AUV) (Jakuba et al., 2014; Jakuba et al., 2018) and Robotically Operated Vehicle (ROV) (Bell et al., 2012) based observing programs referred to in this proposal, are enabling ecological and biogeochemical studies of environments and gradients not accessible by wire-based oceanographic techniques. To date, many of the oxygen sensors used on these platforms were developed for very broad oceanographic applications, and in some cases for very specific oceanographic applications. However there still exists a number of applications for which current commercial systems are poorly optimized, for instance in and around suboxic regions (Hofmann et al., 2011), where oxygen concentrations approach the detection limits of common sensors, and oxygen gradients are particularly high – this can include the environment around submarine hydrothermal vents, oxygen minimum zones in the water column (Stramma et al., 2008), and dead zones in coastal environments. Scientists are now reporting the desire to add more precise oxygen sensing technology onto robotically operated vehicles (Gruber et al., 2010). Thus, there is a need for better matching of oxygen sensing

techniques and methods to applications such as these and, in particular for this thesis, to new vehicle platforms designed to study these environments. In so doing, we can enable both more targeted and higher resolution oxygen measurements than previously possible and potentially use oxygen measurements for a wider range of applications, including *in situ* incubation experiments and primary productivity measurements in the open ocean as well as in shallow marine environments.

Currently, there are several techniques available for measuring dissolved oxygen and an even wider range of specific sensor implementations available for the same (Dick et al., 2016; Wang & Li, 1987). However, these techniques are not all equally well suited to measuring dissolved oxygen on moving oceanographic vehicles. Moreover, not all of these techniques are adaptable to the different constraints of autonomous platforms being developed today.

Efficient matching of measurement methods to deployment platform characteristics requires a careful assessment of the issues involved and also of the implementation of calibration and maintenance techniques in the field. This work has the prospect of refining robotically collected oxygen based measurements in a variety of NOAA relevant applications including during NOAA Ocean Exploration Trust ROV based seafloor surveys (such as the Lo'ihi seamount cruise), during new hydrographic surveys with the *Clio* profiling AUV, and in a range of coastal ocean ecological studies including primary productivity and dissolved oxygen dynamics in the Lower Laguna Madre estuary.

In order to better match oxygen sensors to coastal and open ocean sensing environments, a complete understanding of a sensor's limitations is needed. This is achieved by sensor testing. In this thesis, three sensors were tested in a controlled laboratory setting for various sensor characteristics and statistically compared to one another. The statistical characteristics were

accuracy, stability, detection limit, drift and precision. At the end of the trade study, a summary table was created. This table may then be used for future determination of sensor adaptation.

In order to fully understand all issues involved with deploying and using oxygen sensors in the environment, this project also applied oxygen-sensing technologies in a real world scientific study. This thesis addresses the dissolved/particulate partitioning of Fe emitting from a hydrothermal vent in the Pacific Ocean (Field & Sherrell, 2000a). Hydrothermal vents have become a topic of interest for biogeochemical scientists due to their trace metal and nutrient rich environment (Coale et al., 1991; Toner et al., 2009; Trefry et al., 1985). There are multiple biogeochemical corollaries of microbial activity in seafloor and dark ocean environments (Bach et al., 2006). Oxidation of iron in deep-sea hydrothermal vents is a process that controls the input of this micronutrient to deep-sea ecosystems. The oxidation of dissolved iron from hydrothermal vents is of interest because of the co-precipitation of a variety of vent sourced metals that occurs at vents site contributing to a net sink of certain key trace metals in the ocean chemical budget (Statham et al., 2005). In some hydrothermal settings, such as Lo'ihi seamount, iron oxidation is a major metabolic pathway and geochemical processes that defines the environment (Emerson & Moyer, 2002).

Study Site

A comprehensive set of hydrothermal fluid samples and filters were recovered during a four week long cruise to the Lo'ihi Seamount as part of the NASA funded Systematic Underwater Biogeochemical Science and Exploration Analog (SUBSEA) project. This thesis uses data acquired from cruise one of the SUBSEA project to understand the relationship between dissolved iron and dissolved oxygen at the Lo'ihi Seamount.

Lo'ihi seamount is an extreme environment in key ways: (i) it is suboxic and therefore requires an oxygen sensor with a low detection limit, (ii) it is at a depth of ~1300 m, which the sensor must be capable of operating at, and (iii) the hydrothermal emissions are at the sediment water interface requiring the sensors to be operable very close to the seafloor and robust enough to be manipulated by a remotely operated vehicle. These measurements made at Lo'ihi allow the opportunity to test the understanding of iron oxidation rates in this unique environment, and to more fully evaluate oxygen sensing technologies by comparison to real world observations.

Objectives

This thesis will evaluate oxygen-sensing methods to determine candidate technologies for more optimal integration with robotic and autonomous measurement platforms. This thesis also used ROV based oxygen sensing technologies to evaluate oxidative iron precipitation processes in a deep-sea hydrothermal plume environment. The characteristics of several different oxygen sensing technologies were evaluated, and one was adapted onto a remotely operated vehicle (ROV) based application at the Lo'ihi Seamount. The goal was to identify the best measurement techniques for these applications and develop methods of calibration and operation that result in the most reliable measurements possible.

Hypotheses

There are two major project hypotheses for this thesis:

- There will be proportionally more dissolved iron relative to particulate iron present in the caldera and at the base of the vent sites in the Loihi Seamount. This hypothesis is based on observations that hydrothermal flow in the caldera is low

(Emerson & Moyer, 2002). Additionally, Lo'ihi happens to be located in an oxygen minimum zone.

- This project also hypothesizes that there will be a higher ratio of dissolved to particulate iron in the caldera of the Loihi Seamount as compared to that of other vent sites in the literature (Field & Sherrell, 2000a).

This project tested these hypotheses by analyzing the dissolved iron and particulate iron data collected at the Lo'ihi center caldera using iron concentration detecting colorimetric methods (Viollier, et al., 2000a). The concentrations were converted into dissolved and particulate iron ratios. These results were then used to estimate an approximate iron oxidation rate. This apparent or observed rate was then be compared to other rates in the literature to statistically evaluate the relationship between observed data and theoretical data.

Anticipated Outcomes

Anticipated outcomes of the sensor study were a set of critically evaluated and improved oxygen measurement techniques and operational procedures specific to robotic and autonomous platforms, and collection of high-resolution, high-quality field data from the Hercules ROV testing the application of these techniques in new and novel robotic observing applications. This work also has the potential to lead to the development of a less expensive prototype system that will allow greater flexibility in data collection and lead to improvements in forecasting models. Anticipated outcomes of the scientific study include a kinetic model of dissolved iron as it is emitted from hydrothermal vents and the determination of a relationship between iron and oxygen in the water column.

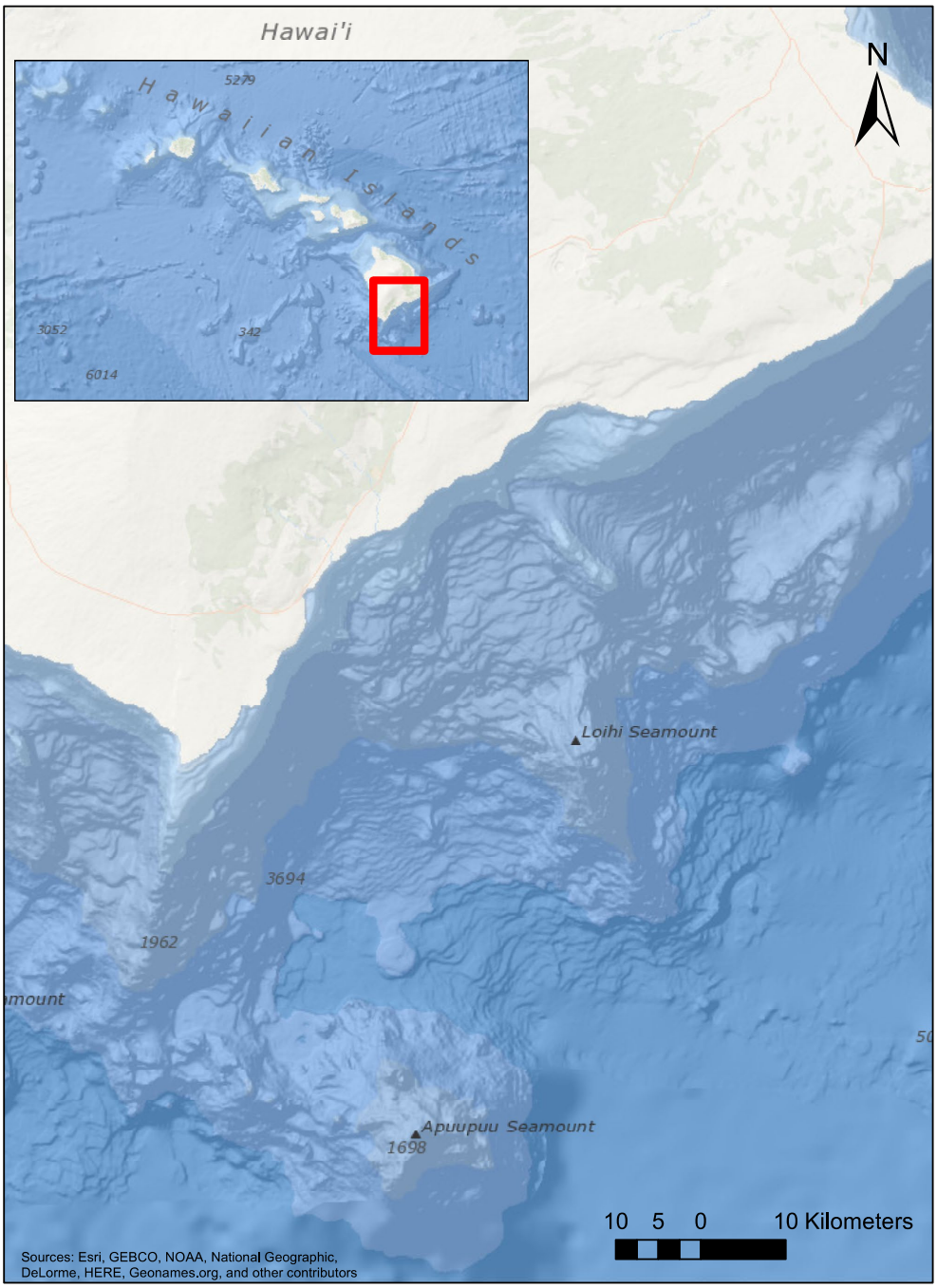

Figure 1. Map of the Lo'ihi Seamount located off the coast of the Big Island of Hawaii

CHAPTER II

OXYGEN SENSORS

Background

Sensors are used to measure a wide variety of parameters. This thesis focuses solely on oxygen sensors and oxygen sensing techniques. Oxygen sensors are widely used to measure the concentration of oxygen in an aqueous solution as an environmental health gauge. Even though the sensors are commonly used in many different aspects of science, they are generally very broad in their sampling range and usually not easily adaptable for various platforms. Roughly within the last decade, there has been an increase in both electrode and optode oxygen sensing studies (Lee et al., 2007; Uchida et al., 2008). This thesis sheds light on the adaptability of oxygen sensors and the many constraints that must be considered in order to adapt an oxygen sensor from one platform to another.

In order to understand the dynamics involved in sensor adaptation and to decide which sensor would best be adaptable for a field test, in-lab sensor characteristic tests were conducted on three different oxygen sensors (shown in Figure 2). Two of the three sensors were optodes and the third sensor was an electrode.

Optodes use optical sensing technologies to produce a measurement. Optodes have been used more and more for oceanic oxygen measurements (Prien, 2007). They typically work by emitting a blue light which excites fluorophores in a chemical polymer sheet that is exposed to

an analyte. The amount of fluorescence being sent back to the detector is proportional to the amount of oxygen in the matrix. Some advantages to using an optode is that it does not consume oxygen when sensing for the measurand and optodes are typically very durable sensors.

The third oxygen sensor tested in this project was a polarographic Clark type electrode. A common amperometric electrode consists of an oxygen permeable membrane covering a platinum cathode. When it is exposed to oxygen the electrode develops a current proportional to the analytic substance being measured. They can be used for studying a wide range of biogeochemical processes (Luther et al., 2008; Taillefert & Rozan, 2002) and have higher resolution as well as lower detection limits compared to optodes. However, they are typically more fragile.

Methods

A series of sensor tests were conducted in order to better understand the operation and usability of different types of oxygen sensors. A posteriori knowledge of the oxygen sensors is vital to ensure that their signals are being interpreted accurately (Kalantar-zadeh, 2013). The tests allowed the sensors to be statistically compared to one another. Statistical characteristics are characteristics that can be measured after the sensors in question have been stabilized at their steady state values (Kalantar-zadeh, 2013). The statistical sensor characteristics tested in this project were stability, short-term drift, precision, accuracy, resolution and detection limit. Each characteristic will be defined for the implementation of this thesis and their measurement acquisition methods will be explained.

2.1 Calibration

In order to conduct the sensors tests, the oxygen sensors were calibrated using either a two point calibration or a one point calibration technique. Typically amperometric sensors require a two point calibration (explained above). Whereas an optical oxygen sensor typically requires a single point calibration (Bell & Dunand, 2010). In this project, the Unisense amperometric oxygen sensor and the neofox optode both used a two point calibrations. The Eureka saunde used a one point calibration. The calibration measurements show the change in the sensor's ability to take a reading over time. This application is crucial for oxygen sensor adaptation because if a sensor is to be mounted onto an autonomous vehicle and sent out to study water quality parameters in a marine ecosystem for more than a few hours, it must be able to remain accurate and dependable for readings throughout that time.

A zero solution was chemically created in the form of a 0.1M solution of sodium ascorbate and NaOH. In order to make this solution, two grams of sodium ascorbate were added to 100mL of water. Afterwhich 0.4 grams of NaOH were added to the mixture and the solution was then allowed to stand overnight so that all oxygen in the matrix can be eliminated. A slight orange pigmentation was shown after the mixture had been allowed time to stand.

2.2 Accuracy

Accuracy is defined as the difference between a sensor's output and the true value of the measurand (Kalantar-zadeh, 2013). For example, a sensor is accurate when the oxygen sensor shows a measurement of 98% dissolved oxygen saturation for an actual 98% dissolved oxygen saturation solution. In order for oxygen sensors to be tested for accuracy, they must be exposed to a solution with a known saturation quantity. This was done by means of measurement

repetitions. The Neofox optode, the Eureka optode and the Unisense electrode were used to measure a known solution of 100% O2 saturation 15 times. These 15 repetitions were recorded and the results for each sensor were shown on a boxplot. Statistical results of the 25th and 75th quantiles were recorded to show the accuracy of each oxygen sensor. The closer the quantile values, the more accurate the sensor.

2.3 Precision

Precision is described as a sensor's ability to reproduce a measurement when testing the same measurand in the same conditions (Kalantar-zadeh, 2013). The sensors were exposed to a known DO value and the sensor reading was recorded. The sensors each took 15 measurements with 7 repetions per measurement. Precision can be assessed from the standard deviation of a set of readings taken by the sensing system (Kalantar-zadeh, 2013). The precision of the sensors was compared by testing multiple sensors (the neofox, the unisense and the eurika). The oxygen sensors were calibrated with known standards (100% and 0% saturation). Afterwhich the sensors were exposed to a known reading and the results for each sensor were depicted in a boxplot along with their respective standard deviation values. The smaller the standard deviation value, the more precise the sensor.

2.4 Resolution and Detection Limit

A sensor's resolution is the smallest detectable change that the sensor can register when testing a measurand. The detection limit of a sensor is the smallest measurable value that a sensor can read and report when measuring a measurand. For resolution and detection limit, this thesis reffers to each sensor's manual. In addition, to the provided data, detection limit was measured by means of a dilution. The dilution saturation percentages tested in this thesis were 100%, 50%, 20%, 10%, 1%, 0.1%. The dilutions used to test for detection limit were 10%, 1%

and 0.1% oxygen saturation. This method proved to be a challenge when testing the eureka optode due to the eureka's additional sensor attachments, slow decrease reading and large size. The unisense electrode and the neofox optode were tested using capped Erlenmeyer flasks typically used for Winkler Titrations (Winkler, 1888). This method was used to reduce the amount of oxygen gas exchange with the environment during the testing period.

Data was recorded for all three oxygen sensors and depicted in the form of boxplots. Nine boxplots are shown, three for each sensor depicting the 10%, 1% and 0.1% oxygen saturation results.

2.5 Short-term Stability

Stability is a sensor's change in precision over a period of time. Stability is similar to a sensor's precision. However, it differs in its definition by the constraint of time being a factor. In order to test for stability, the oxygen sensors were calibrated with known standards (100% and 0% saturation). A known standard was then exposed to the sensor. The oxygen sensor was held in the known saturation solution for 1 minute in order for the sensor to stabilize. A total of 7 measurements were taken per day with 7 repetitions per measurement within a one-minute interval. This was done for each of the three oxygen sensors. The results for all three sensors were plotted and the standard deviation of each of the sensor's readings were recorded to show the stability of the sensors.

2.6 Short-term Drift

Drift is the slow change of a sensor's accuracy over time. Two point calibrations of knonwn standards (100% and 0% oxygen saturation) were used to calibrate the oxygen sesnors in this thesis. Once calibrated, the sensors were repeatedly exposed to an aqueous solution of a known reading of 100% oxygen saturation for a total of two days without recalibration. The results were

graphed by means of a scatter plot with a fitted line added. The slope of the line was then calculated to depict a rate of change or drift in each sensor. Drift is a crucial parameter for understanding the dynamics of an oxygen sensor.

Results

The oxygen sensors tested in this thesis all measured oxygen saturation at standard pressure and the results are expressed in this variable, percent saturation (D'Asaro et al., 2013).

3.1 Precision and Accuracy

The results for precision and accuracy are shown in Figure 4. The graph shows three boxplots, which represent the results for the Neofox optode, Unisense amperometric sensor and Eureka optode from left to right. The measurements were taken in oxygen percent saturation using a known 100% solution for all sensors. The known 100% solution was made by taking deionized Milli-Q water and bubbling it for 10 minutes; then the water was allowed to stand for 5 minutes to prevent super saturation. This technique was used for all known 100% saturation solutions. The Neofox Optode had a 96.4% saturation as its 25th quantile and 114.04% saturation as its 75th quantile value. The Neofox optode also had a 9.58% value for standard deviation. The Unisense amperometric sensor had a value of 100.6% oxygen saturation for its 25th quantile and a value of 102.1% oxygen saturation for its 75th quantile. Additionally, the Unisense sensor had a standard deviation value of 1.01%. Lastly, the Eureka had a 97.7% oxygen saturation value for its 25th quantile and a 98.4% saturation value for its 75th quantile. The Eureka optode had a standard deviation of 0.35%.

3.2 Stability

The results for stability are expressed using Figure 5. The graph shows three linear regressions, which represent the results for the Neofox optode, Unisense electrode and Eureka optode. The measurements were taken in oxygen percent saturation using a known 100% solution for all sensors. The known 100% solution was made by taking deionized Milli-Q water and bubbling it for 10 minutes; then the water was allowed to stand for 5 minutes to prevent super saturation. This technique was used for all known 100% saturation solutions. The Neofox had an average percent saturation reading of 93.25% ±11.07. The Unisense had an average percent saturation reading of 103.09%±1.13. Lastly, the Eureka had an average percent saturation reading of 98.49% ±0.05. Slopes were calculated for the linear regression lines created for each sensor. These slope show a rate of change in stability. The slope for the Neofox optode was -0.001 O_2%sat/min. The slope for the Unisense electrode was -0.021 O_2%sat/min. To conclude, the Eureka had a slope of -0.000 O_2%sat/min.

3.2 Detection Limit

In order to test for detection limit, a dilution series was conducted. Data was recorded for all three oxygen sensors and depicted in the form of boxplots shown in Figure 6. Nine boxplots are shown, three for each sensor depicting the 10%, 1% and 0.1% oxygen saturation results. The Eureka sensor had an r^2 value of 0.783. The Neofox optode had an r^2 value of 0.984. Lastly, the Unisense amperometric sensor had an r^2 value of 0.999. These results indicate that the Eureka optode was the least reliable dilution readings whereas the Unisense oxygen sensor produced the most reliable dilution series readings. The Neofox, although not as inaccurate as the Eureka, was still not as well fitted as the Unisense

3.3 Drift

Drift was measured and recorded by means of a linear regression. The results for drift are shown in Figure 7. The Neofox oxygen sensor showed an average percent saturation of 98.90% ±4.41 with an RSD% of 4.46. The Unisense sensor showed an average percent saturation of 99.08% ±1.38 with an RSD% of 1.39. Lastly, the Eureka oxygen sensor showed an average percent saturation of 98.30% ±1.56 with an RSD% of 1.59. Additionally the slopes for each linear regression are as follows, -0.0001 O_2%sat/min for the Neofox, -0.0004 O_2%sat/min for the Unisense, and 0.0002 O_2%sat/min for the Eureka.

Discussion

Oxygen is a vital ecological health indicator. Thus, oxygen sensors must be reliable and dexterous enough to withstand the many different platforms and environments that the sensor is placed in. In order to have confidence in a sensor's ability to perform, the sensor must be (i) tested in a laboratory setting to ensure proper function and (ii) tested in an extreme setting which allows the sensor to be tested in a more challenging environment. The results of the sensor testing show that the Unisense amperometric oxygen sensor was the most reliable oxygen sensor. Although the Eureka originally showed better precision, it proved to be inadaptable due to its bulkiness and additional sensor attachments. Its abilities were overshadowed by the Unisense electrode's low detection limit, high resolution and high accuracy.

At first, the idea of the Neofox optode was promising. Many articles state the benefits of optical fiber oxygen sensing technologies (Rosenzweig & Kopelman, 1995; Trettnak et al., 1995). The Neofox optode had a chemical patch that would attach to the inside of the sample vile, which allowed for the sample container to remain sealed during the laboratory tests.

This provided the extra comfort of knowing that the water in the sample container was never exposed to atmospheric oxygen after sealing. In many cases, water samples must be tested for oxygen either *in situ*, immediately after collection, or the sample must be fixed to ensure no oxygen gas exchange occurs (Toledo et al., 1981). However, some issues that arose while testing the Neofox optode were that the Neofox oxygen sensor happened to be very temperamental when pressing the sensor up to its chemical "red eye" patch attached to the inside of the sampling container. This led to the Neofox producing results that were not accurate or reliably producible. The Neofox oxygen sensor had poor precision, which could have been due to the sensor's sensitivity to positioning with respect to the chemical patch.

The Eureka optode proved to originally be the most precise and accurate oxygen sensor of the three being tested in this study. However, after testing it became apparent that the Eureka oxygen sensor, although extremely stable and precise, had its drawbacks, such as it was difficult to test during the dilution series. This was due to its extra sensors, large stature, inability to show its original output readings (i.e. millivolt or tau) and inability to accurately measure dilution oxygen solutions.

The Unisense amperometric oxygen sensor proved to be best fitted for adaptation after the conclusion of oxygen sensor characteristic testing. Although it was not as precise as the Eureka at levels of high oxygen saturation and it happened to be extremely fragile, its low detection limit and high resolution made the Unisense electrode the more dependable sensor for adaptation and testing.

Figure 2. Depicts the oxygen sensors referenced in this study. The sensor at the top is the Unisense electrode. The sensor on the left is the Neofox optode, and the sensor on the right is the Eureka optode.

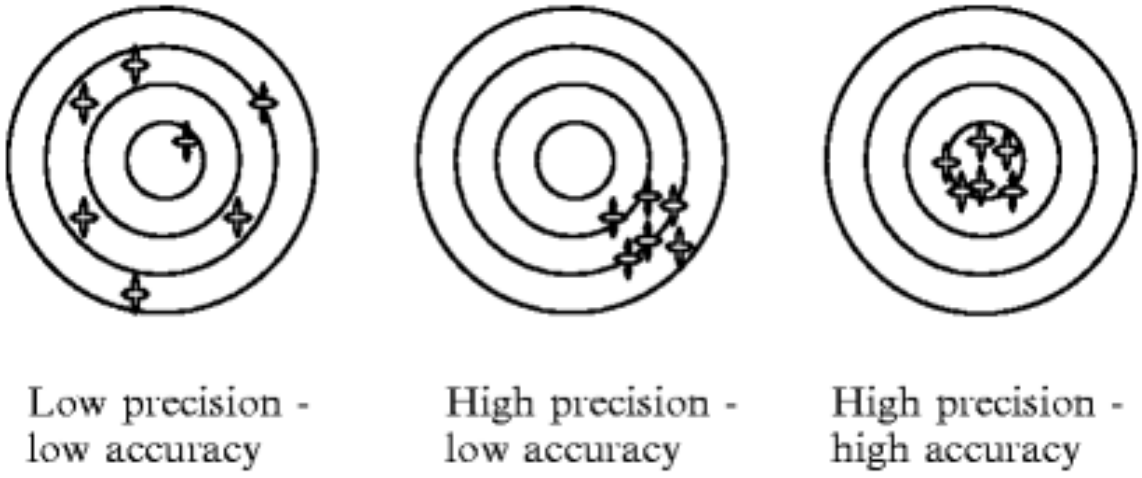

Figure 3. This image depicts the difference between precision and accuracy. The image was taken from Kourosh Kalantar-zadeh's "Sensors: An Introductory Course" (p. 12).

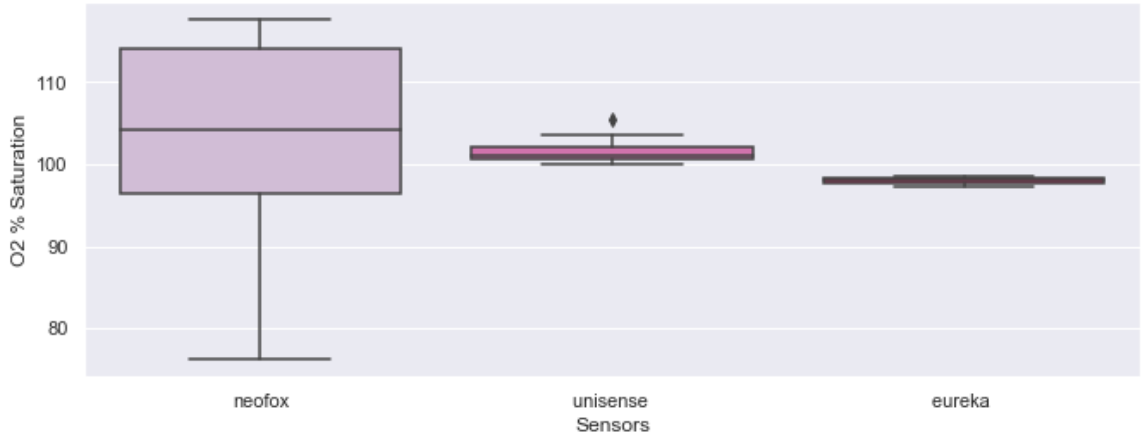

Figure 4. A comparison between the Neofox optode, Eureka optode and the Unisense amperometric sensor. The graphs show the readings for 60 measurements for each sensor. The 25th and 75th quantiles are shown in the box plots for each oxygen sensor.

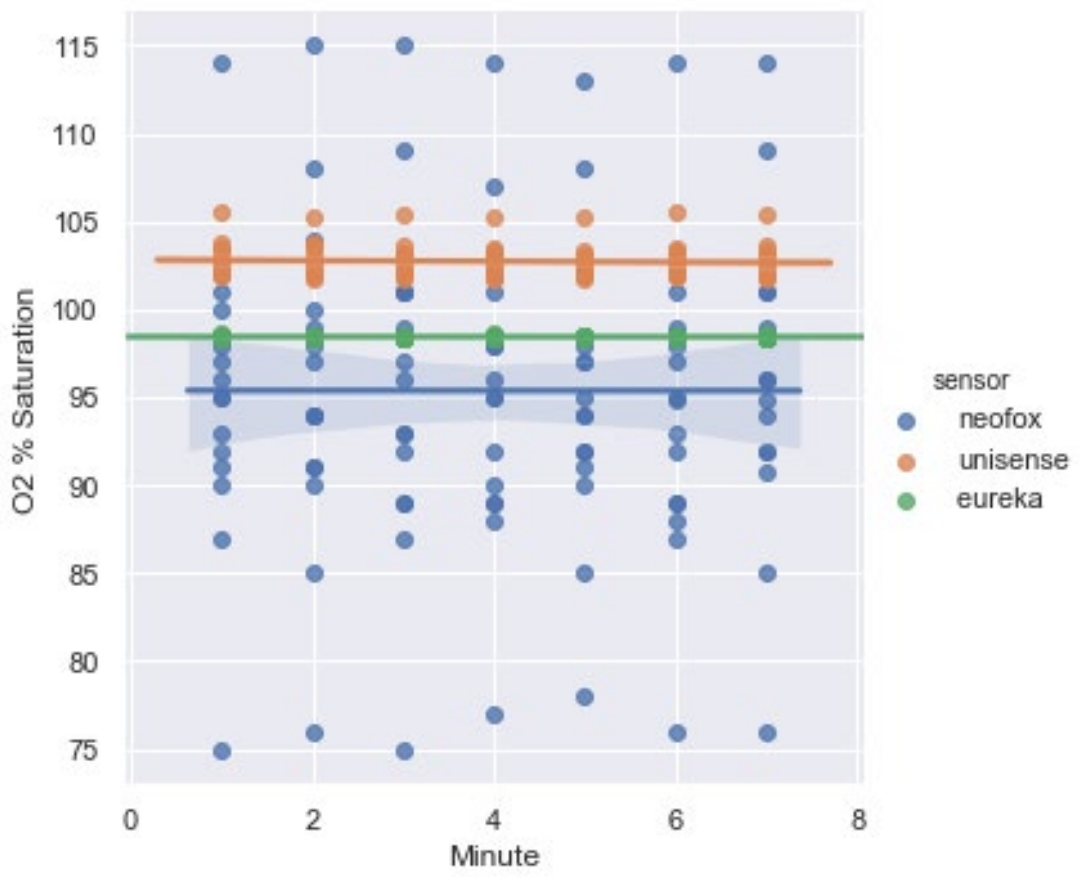

Figure 5. This graph show a scatter plot for the three sensors being tested. The results depict stability.

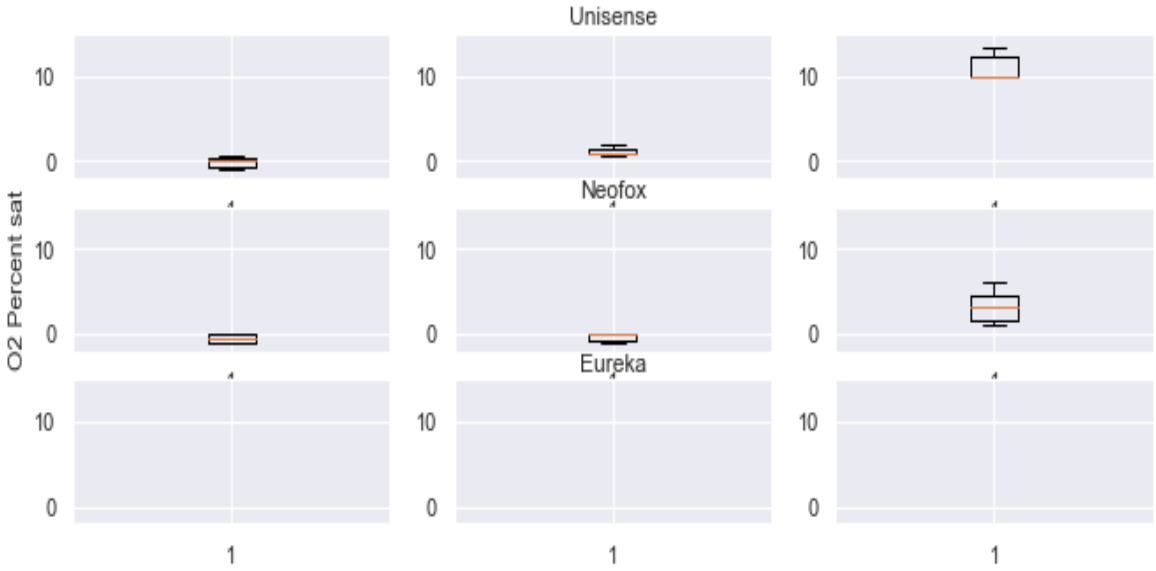

Figure 6. The results for a dilution series test are depicted above. The Eureka optode did not produce results in the scale range.

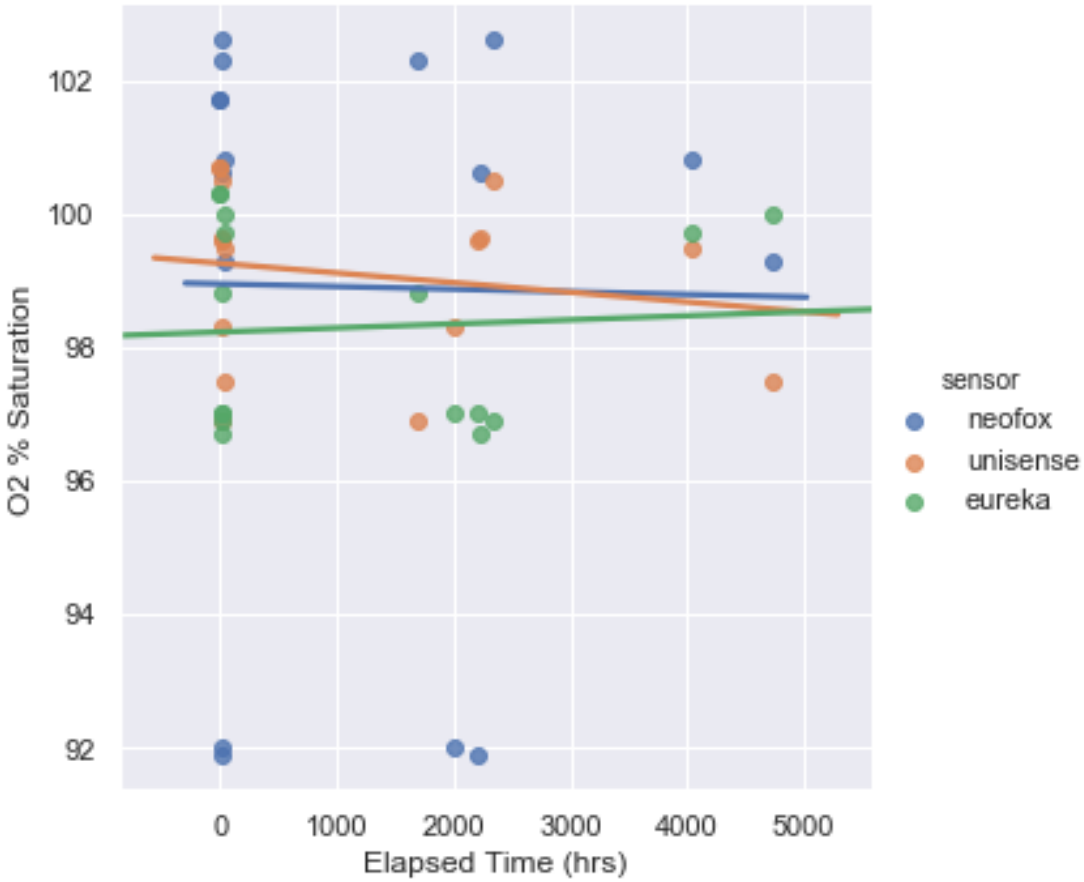

Figure 7. The results for drift are depicted above in the form of a scatter plot. Each sensor was allowed 50 hours without recalibration.

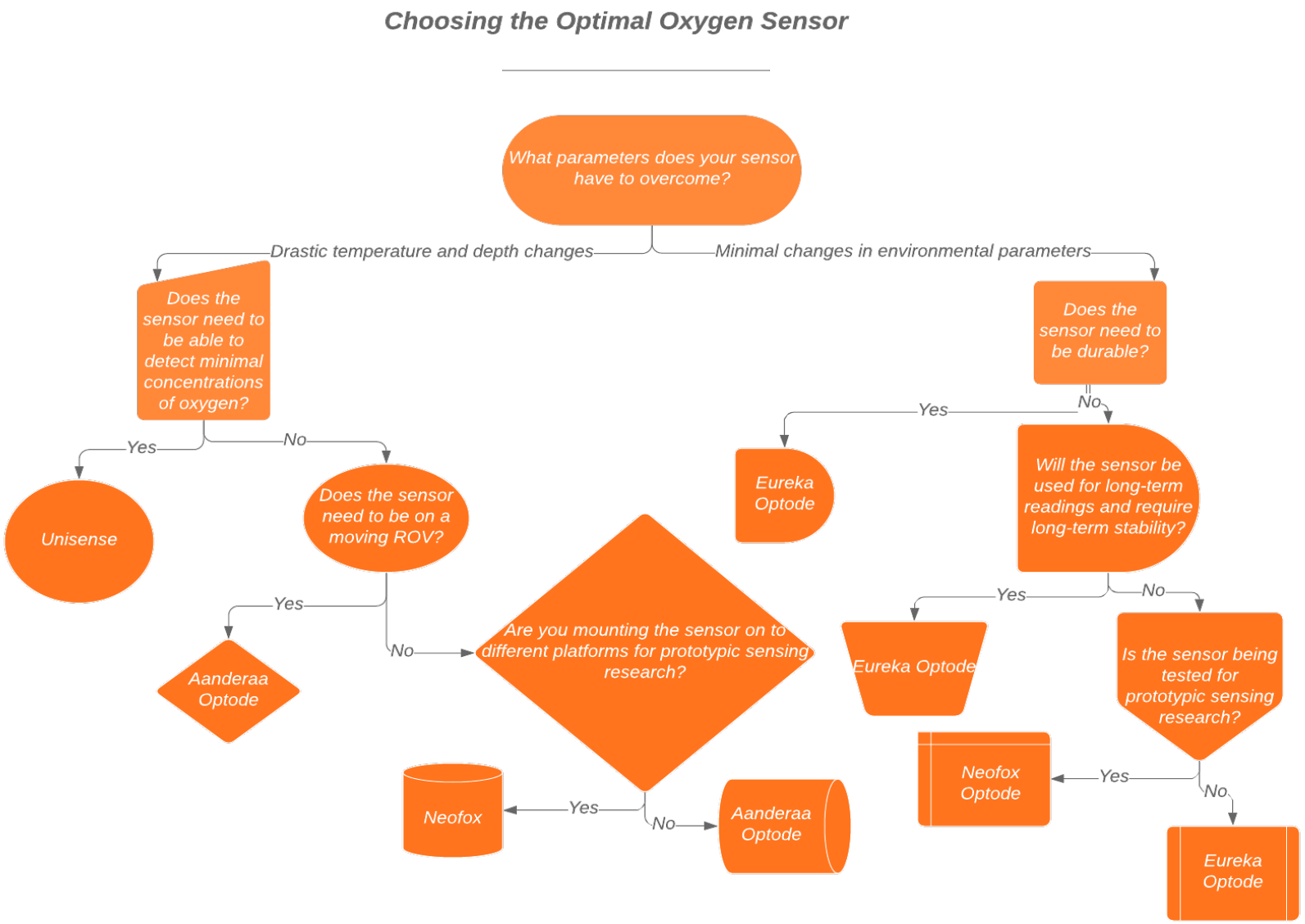

Figure 8. This figure depicts the process of choosing the optimal oxygen sensor.

Table 1. Results for sensor testing and comparison

Sensors	Accuracy (O2% sat)	Precision (SD in O2% sat)	Stability (O2% sat/min)	Drift (O2% sat/hr)	Resolution	Detection Limit	Pros	Cons
Eureka	25th:96.4% 75th:114.0%	0.35	0.000	0.0002	0.1uM	37.28 ± 8.88	Durable	Depth max at 100m
Unisense	25th:100.6% 75th:102.1%	1.01	-0.021	-0.0004	<0.005uM	0.13 ± 0.72	Low detection limit	Physical fragility External electronics attachment
Neofox	25th:97.7% 75th:98.4%	9.58	-0.001	-0.0001	0.1uM	-0.5 ± 0.55	Durable External patch	More specific Requires extra work to achieved good results
Aanderaa*	---	---	---	--	<0.1uM	---	Appropriate depth and detection limit parameters	Less precise measurements

** The Aanderaa optode was not tested in lab. However, it is similar in specs to the Eureka optode*
*** Resolution values for each sensor were collected from the sensor's manual*
**** Detection Limit values are the mean values gathered from each sensor's 0.1% sat results.*

CHAPTER III

IRON OXIDATION STUDY

Background

Iron is the fourth most abundant element on earth (Hauck aat al., 2001). Yet, it is a trace metal in the oceanic environment with average concentration values of 0.05-2.0nM (Wu & Boyle, 1998). It has been stated in literature that iron may be the limiting factor in some oceanic regions (Emmenegger et al., 1998). Most of the iron present in the pacific ocean is released by hydrothermal vents. As dissolved iron leaves a hydrothermal vent entrance, it is exposed to the trace amounts of oxygen in the surrounding water. With the exposure to dissolved oxygen in the water column, dissolved iron is then transformed into its particulate phase. Once it has precipitated out of its dissolved form, it then usually settles back onto the pillow basalt covered sea floor. This causes the vent area to have a distinct yellow-orange pigmentation. This process is the source of a net *sink* for the ocean with respect to iron (Statham et al., 2005). However, not all dissolved iron is precipitated back into the sea floor (Nishioka et al., 2013).

This chapter focuses on the dissolved/particulate partitioning of iron from hydrothermal vents at different depths in the water column (Field & Sherrell, 2000a). In order to study this relationship between dissolved and particulate ferrous iron and the effect dissolved oxygen has on dissolved iron, samples were taken from vent sites at the Lo'ihi Seamount as well as water column samples. Figure 9 depicts the locations of each marker site. The further the ROV travels

away from the plume, the less dissolved iron is expected to be present due to the extended exposure to the trace amounts of dissolved oxygen in the water column. From the samples collected in this thesis, an iron oxidation kinetic model will be calculated. This iron oxidation kinetic model will be studied and compared to known values from the literature to determine the oxidation rate of iron at the Lo'ihi Seamount using statistical comparison methods.

Methods

2.1 Sample Collection

In order to determine the relationship between oxygen and iron at the study site, this thesis used the Suspended Particle Rosette (SUPR) sampler to collect water samples directly from the vents and vertically up the plume (Figure 10). The SUPR sampler is a prototypic sampling system developed by Dr. John Breier (Breier et al., 2009). It is composed of multiple sets of filter stack couplets. Each couplet is composed of a top housing and a bottom housing. In between the two housings there is a space available for a filter. This sampler is unique in that it is able to filter samples *in situ*. Sample was collected by mounting the SUPR onto the ROV Hercules. The sampler was connected to an intake which allowed for more precise plume collection methods. The sampler was also connected to the adapted Unisense oxygen sensors. Hercules was sent to the plume site. Once sample collection began, water from the site was brought in from the intake and first passed through the top housing of one of the filter stack couplets. After it passed through the top housing it is then pushed past a filter in between the two housings where paticulate is collected. After the sample is pushed through the filter it is stored in the bottom housing. Thus whole water, particulate and filtrate are all collected *in situ.* After the entirety of the samples were collected, the ROV Hercules was brought back to surface and the

water samples were stored in a -20 °C freezer while the filters were stored in a -80 °C freezer below deck. After the completion of the cruise the samples were then transferred to the University of Texas Rio Grande Valley Port Isabel Research Laboratory. The sample information can be found in Table 2.

2.2 Acidification

Immediately after collection, the iron present in the sample container begins to react with the oxygen in the sample container and causes the iron to precipitate. In order to re-dissolve the iron back into the sample matrix for measurement, an iron acidification process had to be implemented on the whole water and filtrate samples. The samples were introduced to hydrochloric acid (150ul of HCl for whole water and 300ul of HCl for filtrate). After exposure, the samples were allowed time to dissolved. During this iron dissolving period, the samples were positioned in the sun for a total of five to seven hours a day for a more thorough breakdown. After the samples were completely dissolved, a pH reading was taken to ensure that an optimal acidification pH of two was reached. If the samples did not achieve a pH of two, more HCl was added until the optimal pH was reached. After which, the samples were then ready to undergo the ferrozine method (Stookey, 1970).

2.3 Digestion

For the filters collected on the cruise, an acid digestion was performed. In order to conduct the digestions, savillex PFA digestion vessels were acid cleaned using *aqua regia*. *Aqua regia* was made by mixing a 3:1 molar ratio of hydrochloric acid (HCl) and nitric acid (HNO3). After the vessels were cleaned, an eighth of each filter was cut and placed in digestion vials along with 3ml of HNO3. The vials were sealed and transferred to a hot block. The temperature on the block was raised to 120°C and the samples were left to digest for 4 hours. Then, the

bottles were allowed to cool overnight and heated again. This process of heating was repeated twice for a total of four hotblock digestion sessions. After the filters were fully digested, the vessels were uncapped and were heated to dryness. Then, 5% HCl was added to each vessel and the bottles were recapped and heated to 60°C for one hour. Once the process was completed and the bottles were cooled, the samples were then transferred to acid cleaned, pre-weighed storage containers.

2.4 Ferrozine Method

The ferrozine method is a colorimetric indicator of iron in an aqueous solution. The ferrozine compound reacts with dissolved iron to form a stable magenta complex, which is soluble in water and is a direct determination of the presence of iron (Stookey, 1970). This method was implemented on the samples post acidification. In order to conduct this measurement a standard curve was first made for calibration (Figure 12). The curve showed the linear relationship between the iron concentration reading of a 1 mg/L standard solution and a 0 mg/L blank. This curve was then used to measure concentration of the samples. Once the standard curve was made, the samples were then ready for testing. For the dissolved iron samples, a volume of 25ml of sample was added to a lidded container. Vent samples were diluted for testing. Ammonium hydroxide was added to the samples to increase their pH to a range of 3-5 pH, if needed. Once the pH was within the desired range of 3-5, 0.5ml of Ferrozine Reagent was added to the sample container and the sample was allowed to rest for 5 minutes for the ferrozine reagent to fully react with any iron in the sample. If iron was present in the sample, a color change occurred (Figure 11). After the sample was given time to react with the ferrozine reagent, the solution was placed in a cuvette and inserted into the spectrophotometer. The spectrophotometer then showed a percent transmission reading, a concentration reading and an

absorbance reading for each sample. The values coincided with the concentration of iron in the sample. Once the ferrozine method was completed, the data was recorded and corrected using gravimetric data conversions. The samples testing in this thesis are for particulate iron (P Fe) and dissolved iron (D Fe). These results were used to calculate total iron (T Fe).

2.5 Iron Oxidation

Once T Fe was calculated, the ratio of particulate iron to total iron was shown as a percentage to demonstrate the percent of iron oxidation at depth in the water column (Rouxel et al., 2018). After the iron oxidation percentage was calculated and recorded in table 1, a kinetic model was developed with the observed data. Kinetic models are known in literature to be mechanistic representations of biogeochemical systems (Hasdemir et al., 2014). The iron kinetic rates were calculated by implementing the mathematical techniques used in the literature (Field & Sherrell, 2000b; Millero et al., 1987). Once the iron oxidation rates were calculated, the rates were then compared to known rates in the literature using percent difference.

2.6 Rates and Comparisons

The iron oxidation kinetic rate was calculated by using the iron oxidation kinetic equations in the literature (Millero et al., 1987).

$$-\frac{d[Fe(II)]}{dt} = k_1[Fe(II)] \quad (2)$$

$$k_1 = k[OH-]^2[O_2] \quad (3)$$

After the rates were calculated, they were compared to the literature (Field & Sherrell, 2000b) by means of a statistical percent difference test. This test is indicative of how closely the results of this thesis from samples collected at Lo'ihi compare to those in the literature.

Results

The results for this iron oxidation field study can be expressed in three parts. The first set of results are shown for the ferrozine method. The second set of results expressed in this section show the relationship between iron and oxygen in the water column. The final section shows the comparison between the results acquired in this thesis and the results in other works.

3.1 Ferrozine Method

In order to conduct the ferrozine method, a standard curve was first made to calculate concentration of iron in a sample. This curve made by diluting a 1mg/L standard solution to 75%, 50% and 25% their concentration. The results are shown by comparing the known dilutions to the results from the spectrophotometer absorbance (Figure 12). The standard curve showed a relevant standard deviation percentage (RSD) of less than 5% indicating that the standard curve measurements were within a 95% confidence interval. After the curve was made, the samples were then tested for their respective iron concentrations.

The samples were exposed to a ferrozine reagent, which facilitated a color change in the presence of dissolved iron (depicted in Figure 11). As expected, the samples taken from the vent site had a larger concentration of iron than those taken further up into the water column. For example, a sample taken from the water column, furthest away from the vent site (dive number 1707 sample name S1) showed a total absorbance reading of 0.026, a total percent transmission

of 94.3% transmission and a concentration reading of 0.023 mg/L of iron. These results of iron concentration were then recorded and converted to μmol/L of iron in Table 3.

3.2 Iron Oxidation

The results for iron oxidation are expressed in table 3 as %FeOx. They were calculated by means of particulate iron (P Fe) over total iron (T Fe) and then conveyed in a percentage.

$$\%FeOX = \left(\frac{P\ Fe}{T\ Fe}\right) 100 \qquad (9)$$

This shows the ratio between oxidized iron and total iron. Unexpectedly, the highest percentage of iron oxidation occurred at the marker 2 vent site. Apart from the marker 2 site, the other samples showed a more usual trend with higher oxidation occurring in the water column and lower oxidation values being expressed at the vent sites. These rate results can be seen in Table 3 and are depicted in Figure 14. After the oxidation of iron was calculated an investigation on the rate of oxidation of iron was needed to understand the role that oxygen plays on iron (Stumm & Lee, 1961) . Thus, the results were compared to those in the literature.

3.3 Rate Comparison

The results from Lo'ihi were compared to eight different vent sites in the literature. Table 5 shows the percent difference for Lo'ihi compared to each literature site. Lo'ihi showed an average rate similar to the Juan de Fuca site as well as the Gorda Ridge site from the literature.

Discussion

Literature has stated that complete oxidation of dissolved iron emitting from hydrothermal vents does not occur (Field & Sherrell, 2000a). This project agrees with the literature in this sentiment. In addition, the results from this thesis project support the hypothesis that there was proportionally more dissolved iron relative to particulate iron present in the caldera and at the base of the vent sites in the Loihi Seamount.

Another anomaly noticed was that the marker 2 vent site showed an unexpectedly high amount of particulate iron. Typically, there is a greater amount of dissolved iron present at the orface of a vent site, however the marker 2 site was exhibiting roughly a 98% iron oxidation record. After addressing the literature, it was discovered that at this vent site ferrous iron is progressively being oxidized at the subsurface level which allows for Fe-oxyhydroxide particulate formation and precipitation (Rouxel et al., 2018).

Some challenges that arose while sampling were that during the sample collection period the area was under peak hurricane season. The research vessel had to constantly leave from the sample area in order to keep the vessel and its inhabitants safe. This limited the amount of ROV dives which could be conducted during the sample collection period.

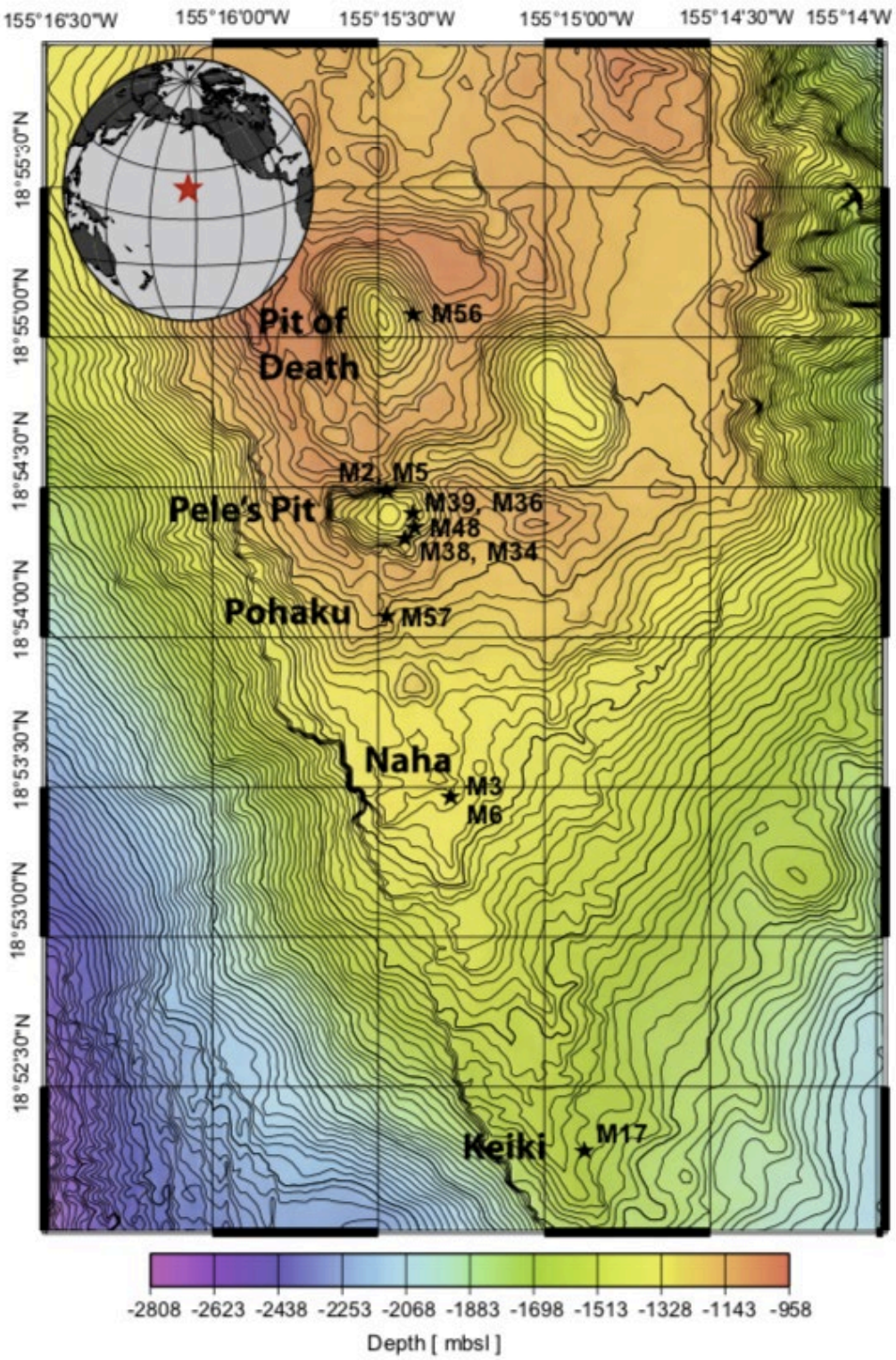

Figure 9. Depicts the sample sites in which the data from this study was collected. The sites mentioned in this thesis are M34, M38, M2, and M57. This image was taken from Rouxel et al., 2017.

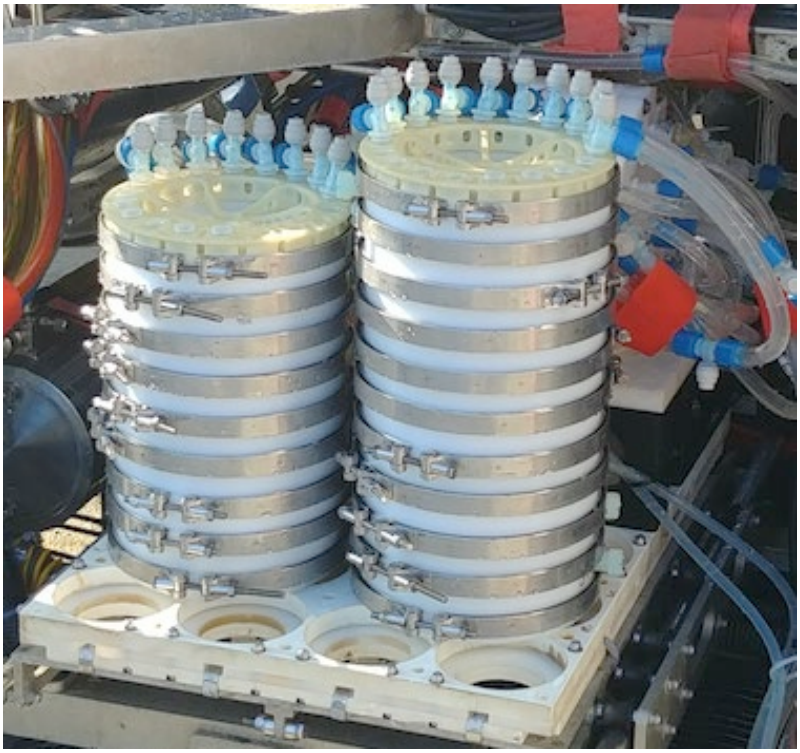

Figure 10. Picture of the SUPR sampler.

Figure 11. Iron sample with color change brought on by the addition of the ferrozine reagent.

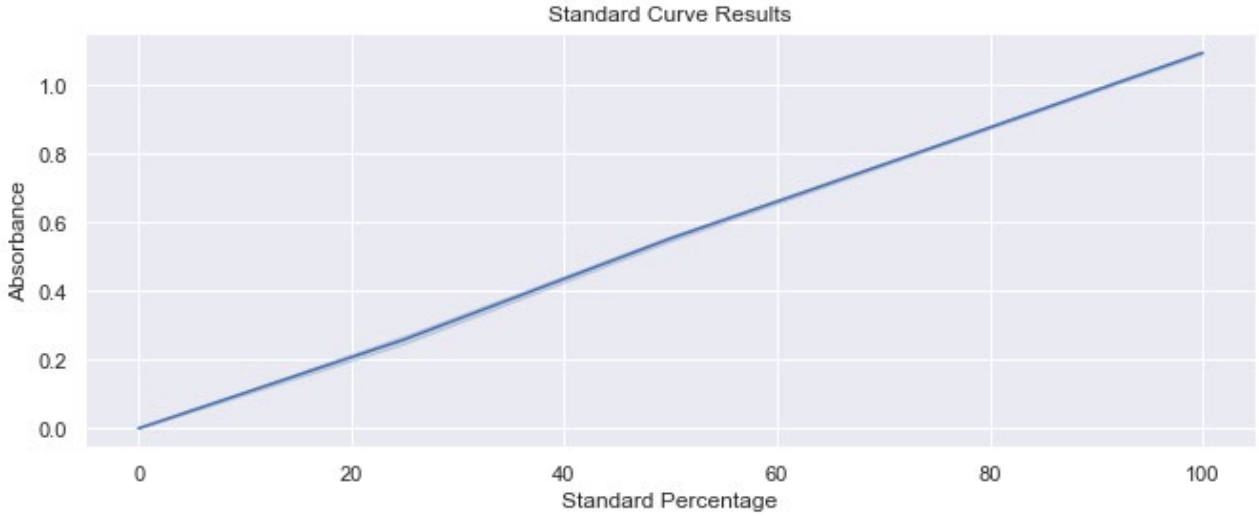

Figure 12. Shows the standard curve expressed in concentration, absorbance, and percent transmission. Also expressed the curve in a relationship between concentration and percent transmission.

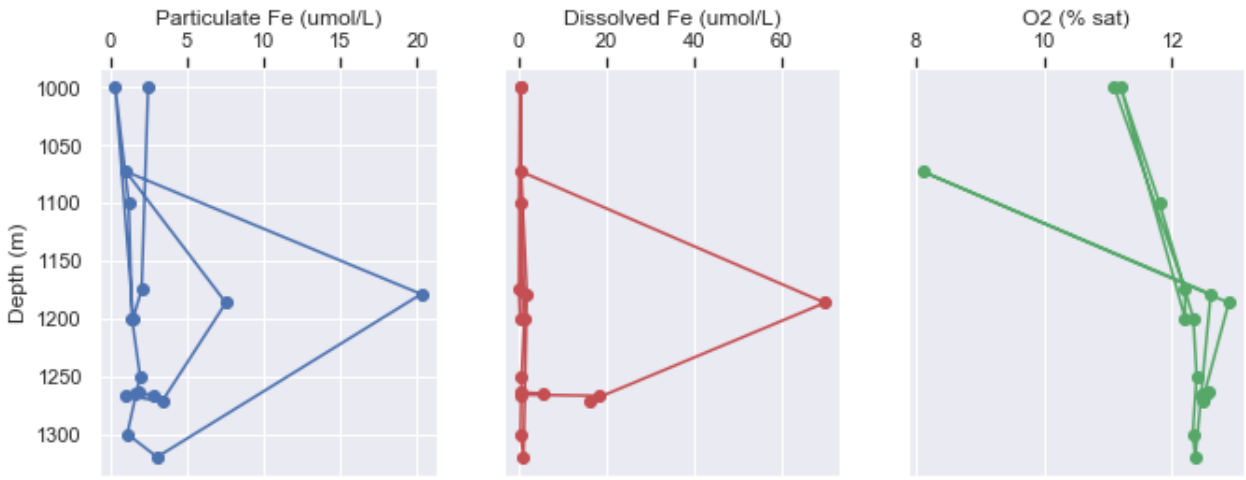

Figure 13. Shows depth comparisons between particulate iron, dissolved iron and dissolved oxygen.

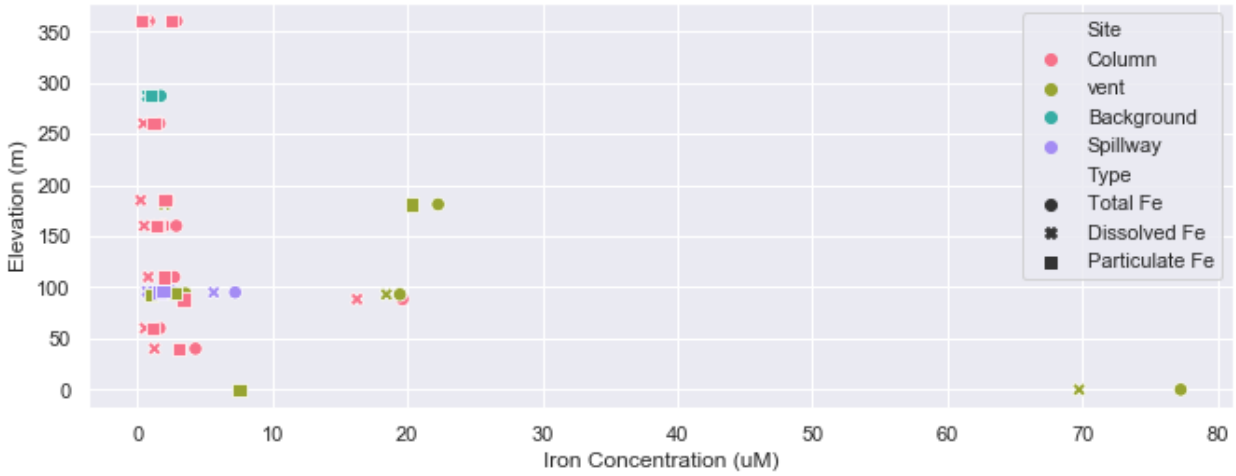

Figure 14. Shows the relationship between iron concentrations from dissolved, particulate and total iron with respect to the site in which the sample was collected.

Table 2. This table shows dive number, site where sample was collected, sample name, sample type, depth, volume filtrated through the system, dissolved iron particulate iron and dissolved oxygen for iron oxidation analysis.

Field	SUPR Tag	Dive	Site	Date Collected	Lat	Long	Time Collected	Depth (m)	Vol (L)	T (°C)	O2 (% sat)
Lo'ihi	S1	1707	Column	9/1/2018	18.9060145	-155.257775	10:58:58	1000	34.12	4.24	11.1
Lo'ihi	S2	1707	Column	9/1/2018	18.90655264	-155.2584594	11:22:37	1175	49.07	3.87	12.2
Lo'ihi	S3	1707	Column	9/1/2018	18.906206	-155.2582455	11:34:36	1200	23.68	3.87	12.2
Lo'ihi	S1	1709	Column	9/3/2018	18.90618802	-155.2576451	11:04:27	1000	64.14	4.26	11.2
Lo'ihi	S2	1709	Column	9/3/2018	18.9069685	-155.258067	11:28:57	1100	60.35	3.99	11.8
Lo'ihi	S3	1709	Column	9/3/2018	18.90698177	-155.258055	11:43:15	1200	32.83	3.85	12.33
Lo'ihi	S4	1709	Column	9/3/2018	18.90694959	-155.2580426	11:54:56	1250	34.91	3.84	12.38
Lo'ihi	S5	1709	Column	9/3/2018	18.9071125	-155.257881	12:07:14	1300	36.12	3.85	12.32
Lo'ihi	S6	1709	Column	9/3/2018	18.907223	-155.2574536	12:23:22	1320	33.08	3.87	12.36
Lo'ihi	S7	1709	M2 Vent	9/3/2018	18.9087645	-155.2574565	16:11:30	1179	35.45	12	12.6
Lo'ihi	S8	1709	Background	9/3/2018	18.92385409	-155.2590255	0:01:03	1073	32.32	6.4	8.12
Lo'ihi	S1	1710	M57 Vent	9/4/2018	18.90132054	-155.258106	13:21:36	1186.5	27.51	11	12.88
Lo'ihi	S4	1712	Column	9/8/2018	18.905622	-155.2568765	12:10:44	1271.7	19.06	40	12.47
Lo'ihi	S5	1712	M34 Vent	9/8/2019	18.90555005	-155.2569817	12:56:13	1267	20.38	39	12.45
Lo'ihi	S6	1712	M38 Vent	9/8/2019	18.90554635	-155.2569826	13:27:30	1266	18.12	15	12.51
Lo'ihi	A7	1712	Spillway	9/8/2019	18.90555073	-155.2569818	13:50:30	1265	19.74	15	12.49
Lo'ihi	S8	1712	Spillway	9/8/2019	18.90554508	-155.2569703	14:12:46	1264	18.68	15	12.57

Table 3. Shows the iron oxidation results for the samples collected at Lo'ihi.

Dive	Site	SUPR	Depth (m)	Vol (L)	T (°C)	T Fe (uM)	D Fe (uM)	P Fe (uM)	O2 (% sat)	O2 (uM)	% FeOx	pH	Ln([Fe])/t (hrs)
1707	Column	S1	1000	34.12	4.28	0.44	0.43	0.0063	11.24	45.69	1.44	7.70	6.72
1707	Column	S2	1175	49.07	3.87	0.23	0.22	0.0059	12.28	50.43	2.61	7.70	6.55
1707	Column	S3	1200	23.68	3.86	0.48	0.48	0.0043	12.31	50.50	0.89	7.70	6.54
1709	Column	S1	1000	64.14	4.27	0.52	0.52	0.0009	11.2	45.54	0.17	7.70	6.76
1709	Column	S2	1100	60.35	3.99	0.43	0.43	0.0036	11.8	48.43	0.83	7.70	6.72
1709	Column	S3	1200	32.83	3.85	1.46	1.46	0.0037	12.33	50.62	0.25	7.70	6.56
1709	Column	S4	1250	34.91	3.84	0.79	0.78	0.0056	12.38	50.89	0.71	7.70	6.49
1709	Column	S5	1300	36.12	3.85	0.54	0.54	0.0031	12.32	50.60	0.57	7.70	6.45
1709	Column	S6	1320	33.08	3.87	1.25	1.24	0.0091	12.36	50.71	0.73	7.70	6.38
1709	M2 Vent	S7	1179	35.45	12	2.05	1.99	0.0605	12.6	51.92	2.95	6.20	4.43
1709	Background	S8	1073	32.32	6.4	0.69	0.69	0.0027	8.12	48.98	0.39	7.70	3.58
1710	M57 Vent	S1	1186.5	27.51	11	69.78	69.76	0.0215	12.88	52.92	0.03	5.52	2.86
1712	Column	S4	1271.7	19.06	40	16.26	16.25	0.0099	12.47	51.08	0.06	7.70	0.33
1712	M34 Vent	S5	1267	20.38	39	18.43	18.43	0.0029	12.45	50.83	0.02	6.04	0.01
1712	M38 Vent	S6	1266	18.12	15	0.79	0.78	0.0080	12.51	51.43	1.02	6.09	0.40
1712	Spillway	A7	1265	19.74	15	5.47	5.47	0.0048	12.49	51.31	0.09	5.99	0.40
1712	Spillway	S8	1264	18.68	15	0.70	0.69	0.0055	12.57	51.67	0.79	5.99	0.40

Table 4. Shows data taken from Field and Sherrell, 2000 for comparison.

Site	Lat	Long	Depth	O2 (umol kg-1)	pH	log(k)	k1	Average Half-life (hrs)
Juan de Fuca	40.50N	135W	1958	64	7.70	14.25	0.0016	6.38
Gorda Ridge	40.50N	135W	2792	102	7.74	14.24	0.0031	3.15
21N EPR	20.00N	110W	2371	108	7.73	14.25	0.0031	3.70
9 45N EPR	10.00N	110W	2372	104	7.75	14.25	0.0033	3.33
SEPR	16.75S	113.33W	2372	153	7.81	14.25	0.0063	1.83
SW Indian R	28.66S	54.50E	3092	178	7.81	14.25	0.0081	1.31
TAG	25.36N	55.90E	3058	254	7.94	14.26	0.0263	0.45
Rainbow	35.99N	47.01W	1942	269	7.99	14.28	0.0398	0.29

Table 5. Shows comparison results.

Site	Average Half-life (hrs)	Lo'ihi Average Half-life (hrs)	Percent Difference (%)
Juan de Fuca	6.38	4.21	0.34
Gorda Ridge	3.15	4.21	0.34
21N EPR	3.70	4.21	0.14
9 45N EPR	3.33	4.21	0.26
SEPR	1.83	4.21	1.30
SW Indian R	1.31	4.21	2.21
TAG	0.45	4.21	8.35
Rainbow	0.29	4.21	13.51

CHAPTER IV

CONCLUSION

Summary

Finding the relationship between particulate and dissolved iron and oxygen in hydrothermal plumes allows for a better understanding of the processes that occur in relatively unknown aquatic areas. Furthermore, there has been a incomplete understanding of iron chemistry in hydrothermal plumes for some time (Field & Sherrell, 2000b). In the iron oxidation field study, there was a higher concentration of dissolved iron present in the samples collected at the base of the vent site. There was also far less dissolved iron present in the samples collected in the water column. This was expected due to the prolonged exposure of dissolved iron to trace amounts of dissolved oxygen in the water column. The Lo'ihi Seamount is located in the oxygen minimum zone, which explains the longer half-life of dissolved iron present at Lo'ihi compared to most of the other sites compared in this thesis.

Broader impacts

The focus of this thesis has been to understand the many constraints that arise from testing and adapting oxygen sensors. In order to comprehend this, three different oxygen sensors were tested in this project: (1) the Neofox optode, (2) the Eureka optode and (3) the Unisense electrode. Of the three, the Unisense electrode seemed the most adaptable for suboxic, environmental platforms due to its low detection limit and high resolution. However, with its

physical fragility and its external electronics, it was not able to accurately take readings during its field adaptation test. Thus, concluding that there currently is not an oxygen sensor well suited for suboxic, hydrothermal environment measurements. The ideal sensor for this task would (1) be physically durable to withstand the environmental conditions, (2) have a high resolution (3) have a low detection limit and (4) be able to compensate for depth, pressure and temperature changes that occur en route to the vent site.

Dissolved oxygen measurements are a fundamental metric for evaluating the health of an ecosystem. However, there has always been an issue of gas diffusion when conducting *ex situ* oxygen measurements (McNeil et al., 1995). In order to eliminate this issue, *in situ* sensing technologies are being better developed and utilized (Buffle & Horvai, 2000). More and more scientists are using oxygen sensors in new ways and on a variety of sampling platforms (Riser & Johnson, 2008). Taking oxygen data in oxygen minimum zones such as the Lo'ihi seamount is also desirable because although many processes are anaerobic, there are still a number of processes that depend on oxygen, such as the oxidation of iron.

REFERENCES

Bach, W., Edwards, K. J., Hayes, J. M., Sievert, S., Huber, J. A., & Sogin, M. L. (2006). Energy in the dark: Fuel for life in the deep ocean and beyond. *Eos, Transactions American Geophysical Union*, *87*(7), 73. https://doi.org/10.1029/2006EO070002

Bell, K., Elliott, K., Martinez, C., Fuller, S., Douillard, B., & Williams, S. (2012). New Frontiers in Ocean Exploration: The E/V Nautilus and NOAA Ship Okeanos Explorer 2011 Field Season. *Oceanography*, *25*(1), 1–68. https://doi.org/10.5670/oceanog.2011.supplement.01

Bell, S., & Dunand, F. (2010). A Comparison of Amperometric and Optical Dissolved Oxygen Sensors in Power and Industrial Water Applications at Low Oxygen Levels (< 5 µg · kg–1). *PowerPlant Chemistry*, *12*(5), 296–303. Retrieved from https://inis.iaea.org/search/search.aspx?orig_q=RN:41073695

Breier, J. A., Rauch, C. G., McCartney, K., Toner, B. M., Fakra, S. C., White, S. N., & German, C. R. (2009). A suspended-particle rosette multi-sampler for discrete biogeochemical sampling in low-particle-density waters. *Deep Sea Research Part I: Oceanographic Research Papers*, *56*(9), 1579–1589. https://doi.org/10.1016/J.DSR.2009.04.005

Buffle, J. (Jacques), & Horvai, G. (2000). *In-situ monitoring of aquatic systems : chemical analysis and speciation*. Wiley. Retrieved from http://old.iupac.org/publications/books/author/buffle.html

Coale, K. H., Chin, C. S., Massoth, G., J., Johnson, K. S., & Baker, E. T. (1991). In situ chemical mapping of dissolved iron and manganese in hydrothermal plumes. *Nature*, *352*(6333), 325–328. https://doi.org/10.1038/352325a0

D'Asaro, E. A., McNeil, C., D'Asaro, E. A., & McNeil, C. (2013). Calibration and Stability of Oxygen Sensors on Autonomous Floats. *Journal of Atmospheric and Oceanic Technology*, *30*(8), 1896–1906. https://doi.org/10.1175/JTECH-D-12-00222.1

Dick, J. J., Soulsby, C., Birkel, C., Malcolm, I., & Tetzlaff, D. (2016). Continuous Dissolved Oxygen Measurements and Modelling Metabolism in Peatland Streams. *PloS One*, *11*(8), e0161363. https://doi.org/10.1371/journal.pone.0161363

Emerson, D., & Moyer, C. L. (2002). Neutrophilic Fe-oxidizing bacteria are abundant at the Loihi Seamount hydrothermal vents and play a major role in Fe oxide deposition. *Applied and Environmental Microbiology*, *68*(6), 3085–3093. https://doi.org/10.1128/AEM.68.6.3085-3093.2002

Field, M. P., & Sherrell, R. M. (2000a). Dissolved and particulate Fe in a hydrothermal plume at 9°45′N, East Pacific Rise:: Slow Fe (II) oxidation kinetics in Pacific plumes. *Geochimica et Cosmochimica Acta*, *64*(4), 619–628. https://doi.org/10.1016/S0016-7037(99)00333-6

Field, M. P., & Sherrell, R. M. (2000b). Dissolved and particulate Fe in a hydrothermal plume at 9°45′N, East Pacific Rise:: Slow Fe (II) oxidation kinetics in Pacific plumes. *Geochimica et Cosmochimica Acta*, *64*(4), 619–628. https://doi.org/10.1016/S0016-7037(99)00333-6

Gruber, N. (2010). Adding Oxygen to Argo: Developing a Global In Situ Observatory for Ocean Deoxygenation and Biogeochemistry. In *Proceedings of OceanObs'09: Sustained Ocean Observations and Information for Society* (pp. 432–441). European Space Agency. https://doi.org/10.5270/OceanObs09.cwp.39

Gruber, N., Doney, S. C., Emerson, S. R., Gilbert, D., Kobayashi, T., Körtzinger, A., … Ulloa Osvaldo. (2010). Adding Oxygen to Argo: Developing a Global In Situ Observatory for Ocean Deoxygenation and Biogeochemistry. *Proceedings of OceanObs'09: Sustained Ocean Observations and Information for Society*, 432–441. https://doi.org/10.5270/OceanObs09.cwp.39

Hasdemir, D., Hoefsloot, H. C. J., Westerhuis, J. A., & Smilde, A. K. (2014). How informative is your kinetic model?: using resampling methods for model invalidation. *BMC Systems Biology*, *8*, 61. https://doi.org/10.1186/1752-0509-8-61

Hauck, S., Benz, M., Brune, A., & Schink, B. (2001). Ferrous iron oxidation by denitrifying bacteria in profundal sediments of a deep lake (Lake Constance). *FEMS Microbiology Ecology*, *37*(2), 127–134. https://doi.org/10.1111/j.1574-6941.2001.tb00860.x

Hofmann, A. F., Peltzer, E. T., Walz, P. M., & Brewer, P. G. (2011). Hypoxia by degrees: Establishing definitions for a changing ocean. *Deep Sea Research Part I: Oceanographic Research Papers*, *58*(12), 1212–1226. https://doi.org/10.1016/J.DSR.2011.09.004

Jakuba, M., Gomez-Ibanez, D., Saito, M. A., Dick, G., & Breier, J. A. . J. (2014). Clio: An Autonomous Vertical Sampling Vehicle for Global Ocean Biogeochemical Mapping. *American Geophysical Union, Fall Meeting 2014, Abstract Id. OS23A-1177*. Retrieved from http://adsabs.harvard.edu/abs/2014AGUFMOS23A1177J

Jakuba, Michael V., Breier, J. A., Gomez-Ibanez, D., Tradd, K., & Saito, M. A. (2018). Clio: An Autonomous Vertical Sampling Vehicle for Global Ocean Biogeochemical Mapping. In *2018 IEEE/OES Autonomous Underwater Vehicle Workshop (AUV)* (pp. 1–8). IEEE. https://doi.org/10.1109/AUV.2018.8729797

Johnson, K. S., Berelson, W. M., Boss, E. S., Chase, Z., Claustre, H., Emerson, S. R., … Riser, S. C. (n.d.). OBSERVING BIOGEOCHEMICAL CYCLES AT GLOBAL SCALES WITH PROFILING FLOATS AND GLIDERS: PROSPECTS FOR A GLOBAL ARRAY.

Oceanography. Oceanography Society. https://doi.org/10.2307/24861005

Kalantar-zadeh, K. (2013). *Sensors : an introductory course*. Springer. Retrieved from https://books.google.com/books?id=rVZDAAAAQBAJ&dq=sensors+an+introductory+course&lr=&source=gbs_navlinks_s

Lee, J.-H., Lim, T.-S., Seo, Y., Bishop, P. L., & Papautsky, I. (2007). Needle-type dissolved oxygen microelectrode array sensors for in situ measurements. *Sensors and Actuators B: Chemical*, *128*(1), 179–185. https://doi.org/10.1016/J.SNB.2007.06.008

Lukas Emmenegger, *, †, D. Whitney King, ‡, Laura Sigg, † and, & Sulzberger†, B. (1998). Oxidation Kinetics of Fe(II) in a Eutrophic Swiss Lake. https://doi.org/10.1021/ES980207G

Luther, G. W., Glazer, B. T., Ma, S., Trouwborst, R. E., Moore, T. S., Metzger, E., … Brendel, P. J. (2008). Use of voltammetric solid-state (micro)electrodes for studying biogeochemical processes: Laboratory measurements to real time measurements with an in situ electrochemical analyzer (ISEA). *Marine Chemistry*, *108*(3–4), 221–235. https://doi.org/10.1016/J.MARCHEM.2007.03.002

McNeil, C. L., Johnson, B. D., & Farmer, D. M. (1995). In-situ measurement of dissolved nitrogen and oxygen in the ocean. *Deep Sea Research Part I: Oceanographic Research Papers*, *42*(5), 819–826. https://doi.org/10.1016/0967-0637(95)97829-W

Millero, F. J., Sotolongo, S., & Izaguirre, M. (1987). The oxidation kinetics of Fe(II) in seawater. *Geochimica et Cosmochimica Acta*, *51*(4), 793–801. https://doi.org/10.1016/0016-7037(87)90093-7

Nishioka, J., Obata, H., & Tsumune, D. (2013). Evidence of an extensive spread of hydrothermal dissolved iron in the Indian Ocean. *Earth and Planetary Science Letters*, *361*, 26–33. https://doi.org/10.1016/J.EPSL.2012.11.040

Prien, R. D. (2007). The future of chemical in situ sensors. *Marine Chemistry*, *107*(3), 422–432. https://doi.org/10.1016/J.MARCHEM.2007.01.014

Riser, S. C., & Johnson, K. S. (2008). Net production of oxygen in the subtropical ocean. *Nature*, *451*(7176), 323–325. https://doi.org/10.1038/nature06441

Rosenzweig, Z., & Kopelman, R. (1995). Development of a Submicrometer Optical Fiber Oxygen Sensor. *Analytical Chemistry*, *67*(15), 2650–2654. https://doi.org/10.1021/ac00111a024

Rouxel, O., Toner, B., Germain, Y., & Glazer, B. (2018). Geochemical and iron isotopic insights into hydrothermal iron oxyhydroxide deposit formation at Loihi Seamount. *Geochimica et Cosmochimica Acta*, *220*, 449–482. https://doi.org/10.1016/J.GCA.2017.09.050

Statham, P. J., German, C. R., & Connelly, D. P. (2005). Iron (II) distribution and oxidation kinetics in hydrothermal plumes at the Kairei and Edmond vent sites, Indian Ocean. *Earth and Planetary Science Letters*, *236*(3–4), 588–596. https://doi.org/10.1016/J.EPSL.2005.03.008

Stookey, L. L. (1970). Ferrozine---a new spectrophotometric reagent for iron. *Analytical Chemistry*, *42*(7), 779–781. https://doi.org/10.1021/ac60289a016

Stramma, L., Johnson, G. C., Sprintall, J., & Mohrholz, V. (2008). Expanding oxygen-minimum zones in the tropical oceans. *Science (New York, N.Y.)*, *320*(5876), 655–658. https://doi.org/10.1126/science.1153847

Stumm, W., & Lee, G. F. (1961). Oxygenation of Ferrous Iron. *Industrial & Engineering Chemistry*, *53*(2), 143–146. https://doi.org/10.1021/ie50614a030

Taillefert, M., & Rozan, T. F. (2002). *Environmental electrochemistry : analyses of trace element biogeochemistry*. American Chemical Society.

Toledo, A. P. P., Carvalho, J. F., Miazaki, E. S., & Souza, J. A. (1981). Determination of dissolved oxygen: a comparison of some already proposed modifications of the winkler method. *International Journal of Environmental Studies*, *16*(3–4), 219–221. https://doi.org/10.1080/00207238108709872

Toner, B. M., Santelli, C. M., Marcus, M. A., Wirth, R., Chan, C. S., McCollom, T., … Edwards, K. J. (2009). Biogenic iron oxyhydroxide formation at mid-ocean ridge hydrothermal vents: Juan de Fuca Ridge. *Geochimica et Cosmochimica Acta*, *73*(2), 388–403. https://doi.org/10.1016/J.GCA.2008.09.035

Trefry, J. H., Trocine, R. P., Klinkhammer, G. P., & Rona, P. A. (1985). Iron and copper enrichment of suspended particles in dispersed hydrothermal plumes along the mid-Atlantic Ridge. *Geophysical Research Letters*, *12*(8), 506–509. https://doi.org/10.1029/GL012i008p00506

Trettnak, W., Gruber, W., Reininger, F., & Klimant, I. (1995). Recent progress in optical oxygen sensor instrumentation. *Sensors and Actuators B: Chemical*, *29*(1–3), 219–225. https://doi.org/10.1016/0925-4005(95)01686-4

Uchida, H., Kawano, T., Kaneko, I., Fukasawa, M., Uchida, H., Kawano, T., … Fukasawa, M. (2008). In Situ Calibration of Optode-Based Oxygen Sensors. *Journal of Atmospheric and Oceanic Technology*, *25*(12), 2271–2281. https://doi.org/10.1175/2008JTECHO549.1

Ulloa, O., Canfield, D. E., DeLong, E. F., Letelier, R. M., & Stewart, F. J. (2012). Microbial oceanography of anoxic oxygen minimum zones. *Proceedings of the National Academy of Sciences of the United States of America*, *109*(40), 15996–16003. https://doi.org/10.1073/pnas.1205009109

Viollier, E., Inglett, P. ., Hunter, K., Roychoudhury, A. ., & Van Cappellen, P. (2000). The ferrozine method revisited: Fe(II)/Fe(III) determination in natural waters. *Applied Geochemistry*, *15*(6), 785–790. https://doi.org/10.1016/S0883-2927(99)00097-9

Wang, H. Y., & Li, X. M. (1987). Dissolved oxygen measuring method. Retrieved from https://patents.google.com/patent/US4921582A/en

Winkler, L. W. (1888). Die Bestimmung des im Wasser gelösten Sauerstoffes. *Berichte Der Deutschen Chemischen Gesellschaft*, *21*(2), 2843–2854. https://doi.org/10.1002/cber.188802102122

Wu, J., & Boyle, E. A. (1998). Determination of iron in seawater by high-resolution isotope dilution inductively coupled plasma mass spectrometry after Mg(OH)2 coprecipitation. *Analytica Chimica Acta*, *367*(1–3), 183–191. https://doi.org/10.1016/S0003-2670(98)00145-7

BIOGRAPHICAL SKETCH

Brianna Ayleen Alanis attended University of Texas Rio Grande Valley from August 2013 to May 2017 and earned a bachelor's degree majoring in Biology. During the last year of her undergraduate career she was able to work for Dr. John "Chip" Breier as an undergraduate research assistant and intern in the aquarium department at the Gladys Porter Zoo. She was accepted as a graduate student under a NOAA CCME Graduate Fellowship at the University of Texas Rio Grande Valley in August 2017. Her focus was in Marine Chemistry, including her own research in studying oxygen-sensing technologies. She completed her masters degree in Ocean, Coastal and Earth Science in December 2019.

Permanent Mailing Address:

35 Bueno Dr.

Brownsville, TX 78520